Biomass Burning and Water Balance Dynamics in the Lake Chad Basin in Africa

Forrest W. Black [1] , Jejung Lee [1,*], Charles M. Ichoku [2], Luke Ellison [3] , Charles K. Gatebe [4] , Rakiya Babamaaji [5], Khodayar Abdollahi [6] and Soma San [1]

1 Department of Earth and Environmental Sciences, University of Missouri-Kansas City, Kansas City, MO 64110, USA; fwbr3d@mail.umkc.edu (F.W.B.); ssaxk8@umkc.edu (S.S.)
2 Graduate Program, College of Arts & Sciences, Howard University, Washington, DC 20059, USA; charles.ichoku@howard.edu
3 Science Systems and Applications, Inc., Lanham, MD 20706, USA; lukecaj@gmail.com
4 Atmospheric Science Branch SGG, NASA Ames Research Center, Mail Code 245-5, ofc. 136, Moffett Field, CA 94035, USA; charles.k.gatebe@nasa.gov
5 National Space Research and Development Agency (NASRDA), PMB 437, Abuja, Nigeria; rakiya.babamaaji@nasrda.gov.ng
6 Faculty of Natural Resources and Earth Sciences, Shahrekord University, P.O. Box 115, Shahrekord 88186-34141, Iran; kabdolla@sku.ac.ir
* Correspondence: leej@umkc.edu; Tel.: +1-816-235-6495

Abstract: The present study investigated the effect of biomass burning on the water cycle using a case study of the Chari–Logone Catchment of the Lake Chad Basin (LCB). The Chari–Logone catchment was selected because it supplies over 90% of the water input to the lake, which is the largest basin in central Africa. Two water balance simulations, one considering burning and one without, were compared from the years 2003 to 2011. For a more comprehensive assessment of the effects of burning, albedo change, which has been shown to have a significant impact on a number of environmental factors, was used as a model input for calculating potential evapotranspiration (ET). Analysis of the burning scenario showed that burning grassland, which comprises almost 75% of the total Chari–Logone land cover, causes increased ET and runoff during the dry season (November–March). Recent studies have demonstrated that there is an increasing trend in the LCB of converting shrubland, grassland, and wetlands to cropland. This change from grassland to cropland has the potential to decrease the amount of water available to water bodies during the winter. All vegetative classes in a burning scenario showed a decrease in ET during the wet season. Although a decrease in annual precipitation in global circulation processes such as the El Niño Southern Oscillation would cause droughts and induce wildfires in the Sahel, the present study shows that a decrease in ET by the human-induced burning would cause a severe decrease in precipitation as well.

Keywords: Lake Chad Basin; biomass burning; water balance; evapotranspiration; MODIS; albedo

1. Introduction

The African Sahel experienced a dramatic decrease in precipitation in the 1960s to the 1980s, which has drastically affected the size of Lake Chad [1]. Lake Chad gained widespread attention from the scientific community and the general public due to its rapid shrinkage from 25,000 km^2 in 1963 to less than 3000 km^2 in 2008 [2]. Lake Chad's shrinkage is significantly detrimental to regional sustainability, because it is an economically important water resource upon which agricultural and fishing activities depend. In a series of surveys interviewing 25,000 households in the southwestern portion of the lake, 59% of the households earned three-quarters of their income from farming, 36% earned income from a combination of fishing and farming, and 5% relied entirely on fishing [3]. A number of factors have been attributed to shrinkage of the lake, including a decrease in precipitation [4], poor water management practices [5], and land use changes [6].

Most of the rainfall in the LCB is immediately lost to evapotranspiration (ET) [7], leaving the region sensitive to precipitation anomalies. Precipitation in the region is bi-seasonal, with wet season monsoonal rains lasting from April to October, and the dry season the rest of the year. The monsoonal rains are driven by the Intertropical Convergence Zone (ITCZ), created by the convergence of trade winds from the northern and southern hemispheres and forming the ascending branch of the Hadley circulation [8]. Precipitation in the Sahel has been shown to be affected by the El Niño Southern Oscillation (ENSO) system, which is a cycle of ocean and atmospheric interaction that produces an irregularly periodic variation in winds and sea surface temperatures over the tropical eastern Pacific Ocean. During El Niño years, the wind pattern associated with the West African Monsoon has been shown to create a dry condition across the Sahel region, leading to precipitation deficits [9]. High variability of rainfall due to these meteorological factors and other regional phenomena contributed to a series of droughts in the 1970s and 1980s, with a gradual trend of annual rainfall recovery occurring since the 1990s contributing to the recovery of Lake Chad [10].

Another factor which has received little attention is the occurrence of biomass burning, whether through wildfires or human-induced burning. Biomass burning has been shown to have significant impacts on the climate by altering land cover and vegetation [11–13], introducing aerosols and trace gases [14,15], and changing land surface characteristics, especially in regard to surface albedo [16,17]. Dintwe et al. [18] examined the effect of fire-induced albedo change on the surface energy balance in sub-Saharan Africa by using Moderate Resolution Imaging Spectrometer (MODIS) albedo data combined with vegetation cover classes and burn products. The short-term effects of albedo change due to burning contributed to an increase in global radiative forcings, of which the magnitudes were much greater than previously thought for regional climate variability in sub-Saharan Africa. Atchley et al. [19] examined the effect of forest fires on surface and subsurface water balance using the hydrological model ParFlow-CLM. The CLM component of the model solved ET using surface energy balance formulation. The study found that fire disturbance in high severity burn sites increased ET and surface runoff, whereas in low severity areas, reduced transpiration from burning was more significant than the increased runoff. Hodnebrog et al. [20] investigated the effect of biomass burning on precipitation in southern Africa using Global Precipitation Climatology Centre (GPCC) precipitation data in conjunction with black carbon and organic carbon measurements from 1850 to 2000. They showed the strong impact of anthropogenic biomass burning particles during the dry season and a reduction in precipitation by 20–30% over much of Africa from 1950 to 2000.

Ichoku's study [21] of biomass burning in northern sub-Saharan Africa (NSSA), showed an increased conversion of shrubland, grassland, and wetlands to cropland from 2003 to 2013. This in turn, affected the amount of biomass burning that occurred, because prescribed burning is one of the primary sources of biomass burning in NSSA. The study also found that areas with relatively high burn activity experienced much higher evapotranspiration and posited a relationship between biomass burning and decreased precipitation. However, there have been no studies specifically in the LCB examining the relationship between human-induced burning and the water cycle.

A large contributor to biomass burning within the LCB is the use of fire to remove vegetative growth at the end of a growing season and the clearing of grassland and savanna for agricultural use. In the early to late dry season (November–March), a patch mosaic burning regime to clear unwanted vegetation is used to clear savanna and woody areas and facilitate clearing land for planting crops. Burning primarily occurs during the dry season when rainfall is at a minimum to clear the wet season's growth or to convert the land for future agricultural use. Smoke byproducts of biomass burning have been known to produce significant amounts of black carbon, carbon monoxide, and carbon dioxide [14]. Furthermore, the resultant ash and charcoal deposition and change in land cover have been known to have a significant impact on surface albedo [16,22,23]. Surface albedo darkening from burning is caused by char deposition that increases the absorption of solar

radiation [24]. Desales [17] found that changes in albedo coupled with a decrease in leaf area index (LAI) and vegetative land cover fraction from burning was linked to convective instability. The cause of this convective instability and precipitation loss is a cooling and drying of the atmosphere, leading to the weakening of upward atmospheric motion during the onset and mature stages of the monsoon.

Biomass burning effects on the water cycle in the Sahel have been addressed to some degree in regard to ET, soil moisture, and precipitation, but conclusive evidence is limited by issues associated with burning and vegetative seasonality [21]. Other studies associating water cycle changes with burning include its effect on soil infiltration rates, surface runoff [25], and soil erosion [26,27]. Previous studies on the water cycle of Sahelian regions have used models focused on terrestrial water storage (TWS) using data from satellites such as Gravity Recovery and Climate Experiment (GRACE) [28–31]. Although such models have helped to bring about great advances in understanding hydrologic dynamics on a climatic scale, their spatial resolution is too coarse for detailed characterizations of burned areas.

Lack of in situ data is largely due to the sparseness of meteorological stations and the fact that existing stations are inconsistent at recording data on a daily or even monthly basis [32–34]. Additionally, installing new stations is difficult in the LCB due to insecurity in the region. WetSpass, which stands for Water and Energy Transfer between Soil, Plants and Atmosphere under quasi-Steady State, is a physically based water balance model that is not as data-intensive as other water balance models [35,36]. Babamaaji [6] demonstrated the effective use of WetSpass in the LCB. One drawback of WetSpass is its inability to calculate water balance more frequently than seasonally. This, however, has been addressed in the newer version, WetSpass-M [36], which was designed specifically to calculate monthly water balance.

There has been little research on using a water balance model to calculate the effect of biomass burning on a hydrological system, especially in a data-scarce region in Africa. In order to accomplish this, the present study investigated burning effects on the water balance in the LCB by incorporating burning parameters such as surface albedo and land cover characteristics of burned areas into a water balance model. The present water balance modeling approach determines how biomass burning affects regional scale water cycles and interprets whether burning would affect the shrinkage of the lake. The time period chosen for this study was from 2003 to 2011 in order to use albedo change from burning, as suggested by [16]. This study investigates the correlation between increased evapotranspiration or increased precipitation due to burning. If there is a correlation, what vegetative land types are most greatly affected? Supposing a continued conversion of other land use types to cropland, what does this imply for water balance in the LCB? To answer these questions, it is necessary to use the model to simulate how burning affects water balance within the LCB, particularly examining water balance changes in vegetative areas. Determining which parameters are affected by burning and the percentage of land use within the study area are also important steps to building a comprehensive model.

2. Study Area

The Chari–Logone catchment (CLC), a sub-basin of the LCB located south of Lake Chad, was chosen for this study because it provides more than 90% of the water input to Lake Chad and is the main driver for the entire lake system [37]. The Chari and Logone rivers provide an average of 1946 mm/year to the lake, whereas direct rainfall contributes a mere 329 mm annually [38]. The spatial extent of the study area is 601,350 km^2, and it is located within the borders of Cameroon, Chad, Central African Republic, and Sudan. The Chari River originates in the Central African Republic, while the Logone river does so on the Adamawa plateau in Cameroon. The catchment lies between 5° N and 15° N at the eastern part of the Sahel (Figure 1). The topography of the CLC is a plain of clayey soils in the northern region and laterite deposits in the south. The CLC is located in the Chad Graben, which formed prior to the upper Jurassic. The stratigraphic sequence of the Chad

Graben is composed of fine and coarse sands along with reddish and gray clays from the Cretaceous period [39].

Ecologically, the area is in the Sudano–Sahelian savanna zone, covered by short grass savannah with a mixture of grasses, shrubs and trees [40]. Since the 1950s, a large proportion of the land cover of the Sahel region had evolved from savanna to agricultural land use [41]. The most significant land use/land cover transformations have taken place after 1975, particularly the dramatic increase in the areal extent of croplands [42]. An overall increase in runoff and erosion rates in the catchment of Lake Chad has been observed in conjunction with decreased vegetation cover, land clearing, and cropland emergence [41,43]. Land clearing has decreased the content of organic matter in the topsoil and enhanced surface crusting, which lead to an increase in runoff [44]. These changes are related to the demographic expansion of cropland and the heightened demand for agricultural production.
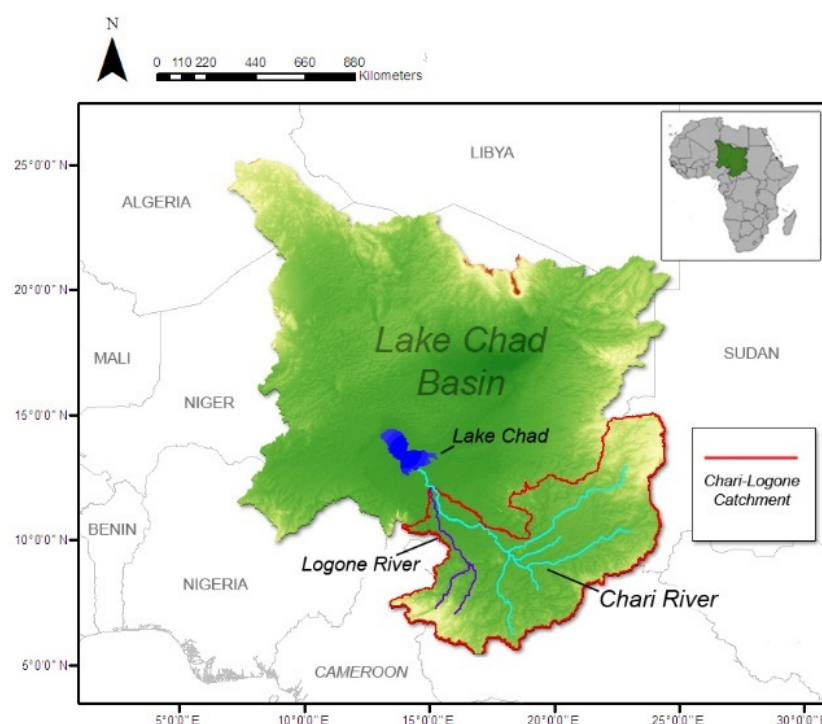

Figure 1. Map of the Lake Chad Basin located in Sahelian Africa. The catchment study region is outlined in red and located in the southeastern portion of the Basin.

3. Materials and Methods

3.1. The WetSpass-M: The Water Balance Model

WetSpass-M utilizes raster data, and calculations are performed on a cell-by-cell basis where the input data are geospatially overlayed and sub-divided into vegetated, bare soil, open water, and impervious surface fractions. Water balance calculations of each pixel are processed in the following order: interception (process 1); surface runoff (process 2); evapotranspiration (process 3); and recharge (process 4) (Figure 2). Additionally, land-use/land-cover fraction values for each pixel are used as weighting factors for the calculation of the water balance [36].

WetSpass-M has demonstrated favorable results for modeling water balance in the western Sahel in the Black Volta Basin [36] and in northern Africa [45]. Calculations for the resolution of the input land cover and soil raster imagery are important to influence sub-cell land cover heterogeneity, because their classification is compared to a series of look-up tables for parameterization during water balance calculations [35]. The look-up tables include land use and land cover, soil type, and rainy days per month. For this study, additional land cover parameters were included in the land use look-up table to

account for burning. These land cover parameters include LAI, vegetated area, burned area, impervious area, open water area, root depth, minimum stomata opening, vegetative height, Manning coefficient, land factor, and aerodynamic resistance. LAI change was calculated using the same method employed by [17], with original unburned vegetation cover, the fractional burned area, and vegetative survival rate as input parameters. Raster datasets required for input into WetSpass-M include precipitation, temperature, wind, soil, land cover, elevation, slope, and potential evapotranspiration (PET). The water balance model outputs are interception, actual evapotranspiration, surface runoff, and recharge, the summation of which are equal to precipitation. WetSpass-M calculates impervious or actual evapotranspiration (ET) using vegetation coefficients in conjunction with PET.
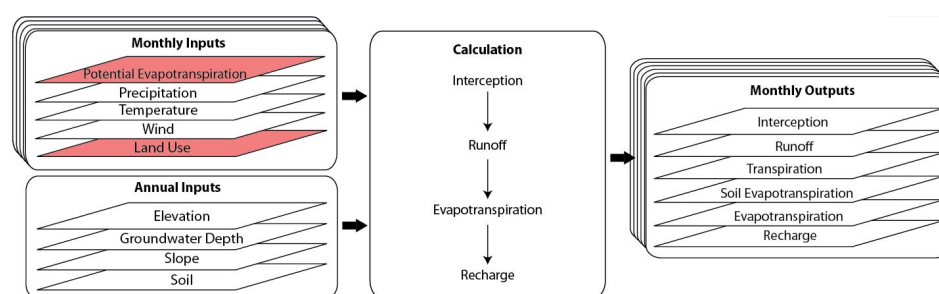

Figure 2. Schematic representation of WetSpass-M inputs and outputs. Data sets shown in red were adjusted to account for burning scenarios.

3.2. Datasets and Parameters for Burning

Ground station observations from the National Oceanic and Atmospheric Administration's (NOAA) National Center for Environmental Information (NCEI) database are available for sub-Saharan Africa. However, the stations in the study area are extremely sparse when compared to the United States or Europe, and monthly or even yearly data are not always recorded for many stations. African stations are also not always accurate, either due to instrument error or poor data management.

With such few ground stations, even if data are accurate, when the data are interpolated across large areas within the study area, they are skewed based on spatial distribution. Therefore, we adopted the precipitation data from the NASA's Tropical Rainfall Measurement Mission (TRMM) https://disc.gsfc.nasa.gov/datasets/TRMM_3B31_7/summary, accessed 17 April 2021. TRMM level 3 3B31 was used for the study, with a 0.5 degree × 0.5 degree resolution at a monthly time scale and units in mm/month. The data cover the area from 40° N to 40° S latitude, and were collected from January 1998 to April 2015, shortly before the satellite re-entered Earth's atmosphere. A number of studies have examined the accuracy of TRMM data compared to station data in different regions [46,47]. One such study by Ojo and Omotosho [48] looked specifically at the accuracy of TRMM in Nigeria. The study found that TRMM performed very well when compared to the few meteorological stations available. TRMM did, however, have a tendency to marginally overestimate precipitation, especially toward southwestern Nigeria, which is far from the study area.

Soil rasters were extracted from the United Nation's Food and Agriculture Organization (FAO) Harmonized World Soil Database (HWSD). The HWSD was released in 2008, and is a 30 arc-second raster database with over 16,000 different soil mapping units that combine existing regional and national updates of soil information worldwide. Land cover data were derived from MODIS MCD12Q1 Collection 6. This Level 3 dataset is a land classification raster created from an algorithm combining data from the Moderate Resolution Imaging Spectrometer (MODIS) instrument onboard NASA's Terra and Aqua satellites. These satellites were launched December 1999 and May 2002, respectively. An advantage of MODIS is its ability to cover the entire globe every 1–2 days with a 2330 km wide swath. MODIS has thirty-six discrete spectral bands, ranging in wavelength from 0.4 μm to 14.4 μm, thereby allowing the retrieval of a wide variety of geophysical prod-

ucts [49,50]. MODIS data have widely been used and validated in a number of studies involving Africa [21,51–53]. MCD12Q1 is available yearly at a 1 km × 1 km resolution. The yearly availability of MCD12Q1 makes it preferable in this study over Globcover, which has shown better performance in Africa although only provides data from December 2004 to June 2006 and January to December 2009 [54].

The MCD12Q1 data are divided into eighteen distinct land classifications, which were converted into another set of classifications required by WetSpass-M. Of the eighteen MODIS classifications, only ten were found in the study area. A model was built in ArcGIS to convert the numbers signifying those ten MODIS classes into eight WetSpass-M classes (Table 1).

Table 1. Conversion table of MODIS land cover class values to WetSpass-M class values.

MODIS		WetSpass-M	
Label	**Number**	**Label**	**Number**
Rainfed Cropland	12, 14	Agriculture	21
Mosaic Vegetation	12, 14	Reference Grassland	307
Forest	6, 7	Mixed Forest	33
Shrubland	6, 7	Shrub	36
Grassland	9, 10	Reference Grassland	307
Sparse Vegetation	9, 10	Reference Grassland	307

Two different land cover datasets were created, one considering burning and one without burning. The dataset considering burning combined the land classification raster with fire counts derived from MOD14/MYD14 Collection 5 fire data. MOD14 data are derived from a fire detection algorithm which takes the two 4 μm channels, numbered 21 and 22. Classification of a pixel as containing fire is only considered if it satisfies a variety of conditions which indicate a strong probability that it contains fire [55,56]. For each grid cell, Terra/Day or Terra/Night settings were selected based on which had the most fire detected; this value was then used for the day. Each daily total was then summed in order to obtain a monthly value per grid cell (Figure 3a,b). Although the monthly value represents one overpass per day, the data are not quantitatively representative of the diurnal burn pattern, however do provide statistically qualitative information. The fire data were then overlaid onto the land cover map using GIS to simulate which vegetated areas were likely affected by burning.

A GIS model was built, which first extracted the fire count for the desired month, and then a raster of only pixels detecting fire was created using the Raster Calculator tool. Specific land cover types were extracted from the previously created yearly land cover data used in the non-burning WetSpass-M model. The extracted land cover classes were cropland, savanna, mixed forest, deciduous forest, coniferous forest, and grassland (Figure 4a). Each land cover area was then used as a mask to extract only those areas which experienced burning. For example, a new raster for savanna was created, only showing those areas in the savanna in which fire was detected for a particular month. Each of the newly created land cover rasters was then assigned a number corresponding to a WetSpass code used in the look-up table. Savanna and grassland were distinguished due to savanna containing more woody vegetation. The difference in vegetative cover affected the parameters used in the look-up table [Table S1]. For example, land cover roughness and vegetative height are higher in savanna areas. The burned areas were merged with the other land cover types such as urban, bare soil, etc., and new classes were assigned to vegetated areas indicated as burned: burned coniferous, burned deciduous, burned mixed forest, burned savanna, and burned grassland (Figure 4b). The land cover values were then used by WetSpass-M to assign land use parameters by means of a look-up table used in water balance calculation.
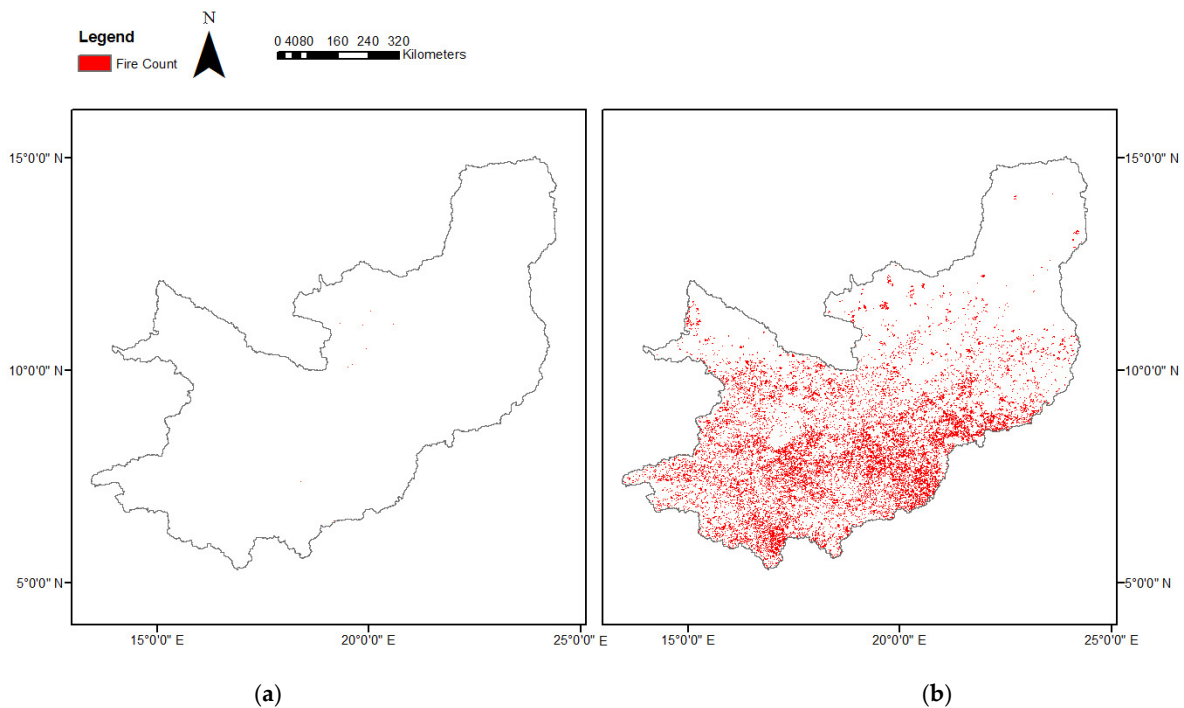
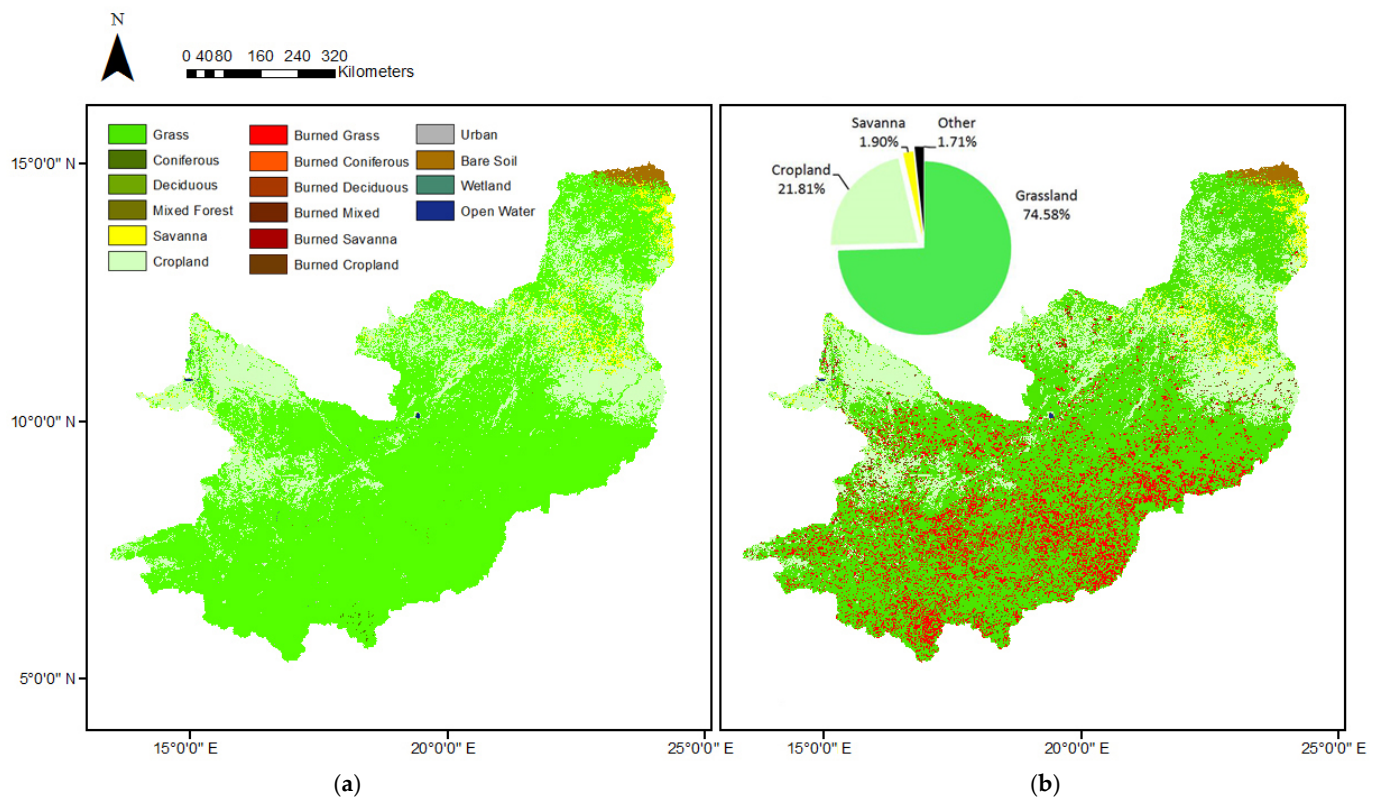**Figure 3.** MOD14 fire counts from the wet season in August 2010 (**a**) and burning season month, January 2010 (**b**).

Figure 4. (**a**). Map showing August 2010 WetSpass-M land cover classifications derived from MODIS MDC12Q1. (**b**) Map showing January 2010 WetSpass-M land cover classifications derived from MODIS MDC12Q1 superimposed with fire detections (red dots) derived from MODIS MOD14. Pie chart shows land cover percentages in the Chari–Logone catchment area derived from MDC12Q1. Grassland is by far the greatest land cover type, followed by cropland. All other land cover types, such as forest, bare soil, wetland, urban, and open water, are combined into the category "other".

For this study, additional land cover types were included in the land use look-up table to account for burning. For example, LAI (the quantity of leaf coverage compared to ground surface area) changes in the look-up table parameters were calculated using the same method employed by [46], with modification of the equation:

$$VC = VC_U[1 - FBA \times (1 - SR)] \tag{1}$$

where VC is the burned vegetation cover, VC_U is the original (unburned) vegetation cover, FBA is the fractional burned area, and SR is the survival rate. Relevant land cover parameters include LAI, vegetated area, burned area, impervious area, open water area, root depth, minimum stomata opening, vegetative height, Manning coefficient, land factor, and aerodynamic resistance. LAI is a quantity, measuring the leaf area per unit of ground surface area. LAI modifies the amount of water from precipitation and heat fluxes, affecting ET and runoff. Minimum stomata opening refers to the minimum size of stomata for that land cover type. Stomata, which are the pores on leaves used for gas exchange, have been shown to change size with temperature and depending on water availability [57]. Burning also reduces canopy height as land is cleared of vegetation, and thus increases wind speed. Increased wind speed reduces sensible heat, increasing leaf temperature and stomatal resistance, thus increasing transpiration. Conversely, decreased vegetative height tends to decrease aerodynamic resistance, also known as drag. Aerodynamic resistance is calculated for the WetSpass-M table using:

$$r_a = \frac{1}{K^2 U_a Z_a}\left(ln\left(\frac{Z_a - Z_d}{Z_0}\right)\right)^2 \tag{2}$$

where r_a is the aerodynamic resistance, K is the von Karman constant (0.41), U_a is the wind speed at elevation Z_a, Z_d is the zero-displacement elevation, and Z_0 is the aerodynamic roughness height of the surface [35]. Decreased aerodynamic resistance has the effect of decreasing ET [58].

Analysis of land use model inputs for the CLC show the dominant classes to be grassland (74.88%), cropland (21.81%), and savanna (1.90%). Coniferous, deciduous, and mixed forest combined only make up 0.12%, with wetland covering 0.2%. Non-vegetative cover are open water (0.28%), urban build-up (0.18%), and bare soil (0.93%) (Figure 4b). Burning within the dominant land cover types showed grassland to have the highest fire detection, with an average of 5–20% of grassland showing fire during the dry season. Grassland fires may be due to controlled burning or wildfires, but that they make up such a large portion of the catchment is significant. Peak burning appears to occur from November to January for all classes, with little to no burning occurring from May to July (Figure 5).
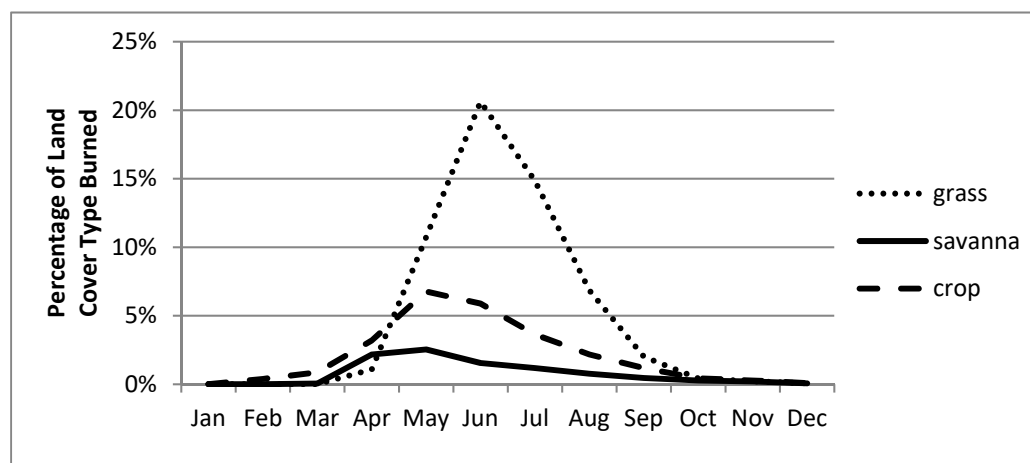

Figure 5. Average percent of monthly burning for major land cover types from 2003 to 2011 taken from MOD14.

Temperature data were extracted from the MOD11C3 Version 5 monthly daytime CMG land surface temperature product from MODIS Terra. MOD11C3 is derived from the MOD11C1 daily global product, taking daily clear sky land surface temperature values and averaging them for one month at a 0.05 degree resolution (~5.56 km). Validation of MODIS land surface temperature has been well researched [59–61]. Hulley and Hook [62] showed the high degree of MODllC1 accuracy in Africa by comparing the data to in situ measurements taken in Namibia, Botswana, and South Africa. MODllC1 Version 5 showed a mere 1.93% combined mean temperature difference from ground measurements. Analysis of land surface temperature showed a decrease in temperature during the wet season due to the cooling effect of precipitation over land.

Global climate models and datasets, such as the NOAA Global Forecast System (GFS) or the NASA Modern-Era Retrospective analysis for Research and Applications (MERRA), provide the wind speed at various atmospheric layers. Unfortunately, GFS has a relatively low resolution of 28 km, which is far too coarse for this study. Mesoscale models such as the Weather Research and Forecasting (WRF) model could be configured for the study area. However, this was beyond the scope of the study and, even then, such models have difficulty accounting for the complex terrain when calculating near-surface winds at a desired resolution [63,64]. For these reasons, station data were used for the wind speed, despite issues with data continuity. NOAA does not provide monthly wind speed averages, therefore daily records from NCEI Global Summaries of the Day were used and averaged monthly. The average wind speed values were also converted from 0.1 knots to m/s. Once the wind speed data were averaged, they were imported into ArcGIS as a shapefile and converted to rasters using kriging [65]. The data were then processed and converted into the proper format for input into WetSpass-M.

PET is the maximum evaporation and transpiration that could occur, assuming sufficient water. As noted earlier, burning has a significant impact on surface albedo change. This change in albedo affects the energy balance and therefore should not be overlooked when calculating PET. Two PET datasets were created for use with the two WetSpass-M models. Albedo values considering burned and non-burned vegetative classes were derived from [16], and those of non-vegetative areas were taken from Yu and Lu [66]. The spatial distribution of albedo was assigned using the modified MDC12Q1 (Type1) yearly land cover data showing burned areas. To consider the effect of albedo change on PET, a simplified Penman equation was used, following the method outlined by Valiantzas [67]:

$$E_{PEN} \approx 0.051(1-\alpha)R_S\sqrt{T+9.5} - 2.4\left(\frac{R_S}{R_A}\right)^2 + 0.052(T+20)\left(1-\frac{RH}{100}\right)(a_u - 0.38 + 0.54u) \tag{3}$$

where E_{PEN} is the Penman potential evapotranspiration, α is the albedo, R_s is the solar radiation, T is the surface temperature, R_A is the extraterrestrial radiation, RH is the relative humidity, a_u is a wind function coefficient of 1, and u is the wind speed. The wind coefficient of 1 was originally used by Penman [68]. No solar radiation information was available from regional station data; therefore, it was estimated from measured sunshine hours using the equation:

$$R_S = R_A \times \left(0.5 + 0.25 \times \frac{n}{N}\right) \tag{4}$$

where n is the measured bright sunshine hours per day, and N is the maximum possible duration of daylight which is derived from the latitude of the site and the number of the Julian months [69,70]. R_A is calculated using:

$$R_A = 37.59d_r[\omega_S \sin(\phi)\sin(\delta) + \sin(\omega_S)\cos(\phi)\cos(\delta)] \tag{5}$$

where d_r is the relative distance between the sun and the earth, ϕ is the latitude in radians, and δ is the solar declination. The maximum possible duration of daylight was calculated using the equation:

$$N = \frac{24}{\pi}\omega_S \tag{6}$$

where ω_S is the sunset hour angle in radians. δ is the solar declination and is determined using:

$$\delta = 0.409 \sin\left(\left(\frac{2\pi}{365}\right)J - 1.39\right) \tag{7}$$

where J is the Julian day corresponding to the respective month [69,70]. Relative humidity was calculated using the equation:

$$RH = 100\left(\frac{e_a}{e^\circ(T)}\right) \tag{8}$$

where $e^\circ(T)$ is the saturation vapor pressure (kPa) and e_a is the actual vapor pressure.

Climate station data from NCEI Global Summaries of the Month were used to calculate solar radiation, extraterrestrial radiation, and relative humidity; these values were used to create raster datasets. The data were imported into GIS and a model was used to calculate the two PET datasets and export them for use as WetSpass-M inputs. PET was validated by comparing the calculated PET to the Consultative Group for International Agricultural Research (CGIAR-CSI) PET, which averaged PET observations from 1950 to 2000 [71,72]. Calculated PET with albedo matched well against the CGIAR PET [Figure S1].

Elevation from a digital elevation model (DEM) was provided by the Shuttle Radar Topography Mission (SRTM). The Shuttle Radar Topography Mission (SRTM) is an international project coordinated by the National Imagery and Mapping Agency (NIMA) and NASA [73]. The primary objective of the mission was the acquisition of a complete, high-resolution, digital topographic database of the Earth. SRTM, which flew onboard the Space Shuttle Endeavour, consisted of a specially modified radar system and had an 11-day mission in February 2000. The digital topographic map products were designed to meet Interferometric Terrain Height Data (ITHD) specifications, with 30 m × 30 m spatial sampling and absolute vertical height accuracy (90% linear error) of 16 m. The absolute horizontal accuracy (90% circular error) was 20 m. The SRTM resolution used in this study was 90 m × 90 m [74]. The slope was calculated using the elevation input by the WetSpass-M program.

Finally, a groundwater raster dataset was generated using 2009 measurements taken from a collaborative study in the Lake Chad Basin by the University of Missouri, Kansas City and NASA Goddard Space Flight Center and [75]. The data were imported into ArcGIS and converted to shapefile points and converted to raster using kriging. These same data were used by Babamaaji [6].

4. Results

4.1. Validation

We performed model validation by comparing runoff outputs from WetSpass-M to the Logone river discharge measurements acquired at the Bongor station from 2003 to 2007 [76]. A Nash–Sutcliffe efficiency (NSE) value of 0.57 was found for the datasets, indicating that the model did well in calculating hydrological parameters (Figure S2a), where a value between 0 and 1 is considered good with 1 being the perfect match [77]. An r^2 value of 0.68 (Figure S2b) found between the measured and calculated value was satisfactory.

4.2. Analysis

Analysis of the model results considering albedo change from burning showed the majority of precipitation being distributed to ET and recharge. The majority of available water from precipitation was lost to ET (45.19%) and groundwater recharge (45.35%), leaving a smaller portion available for surface runoff. We determined the burning impact by subtracting the monthly average outputs without burning from those with burning for 2003 to 2011.

To obtain a more detailed understanding of fire effect in the CLC, an investigation of the effect of fire by land cover type was performed. Particular attention was paid to the three primary land cover classes in the study area: grassland, savanna, and cropland. Average wet season ET decreased 6.44 + 03 mm per month, and decreased 2.01 + 02 mm per month for the dry season. This is in agreement with other studies [78,79], which found that ET was especially reduced by burning during the early monsoonal season. Increases in ET, recharge, and runoff due to fire were observed in the dry season and can be attributed primarily to grassland burning (Figure 6a,b). Considering burning, grassland showed an increase in ET and recharge during the dry season, but showed a decreasing pattern in the wet season. These parameters have increased runoff during the wet season (Figure 6b).

Considering no burning, there was more ET observed during the wet season in the savanna, whereas there was less ET, more runoff, and more recharge when considering burning (Figure 6c). Cropland showed more runoff, but less recharge and ET during the wet season (Figure 6d).
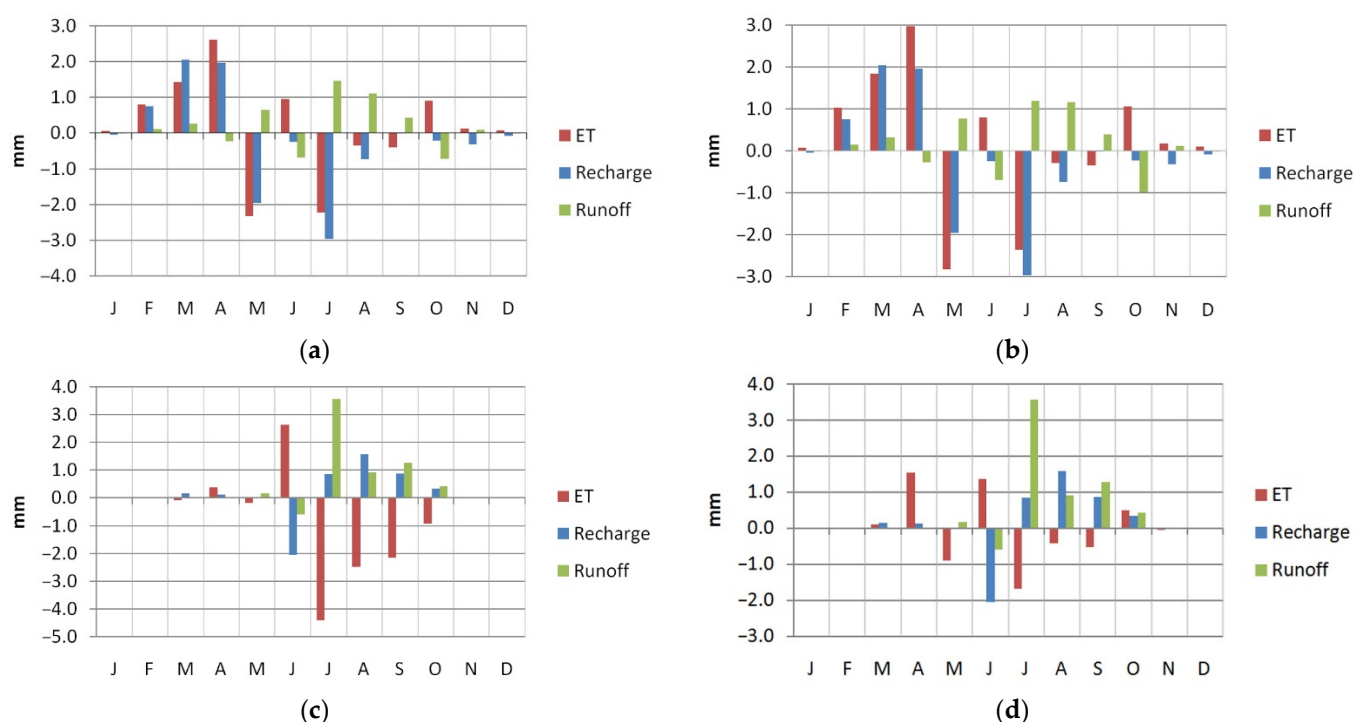

Figure 6. Average monthly output difference of hydrological parameters from the non-burning model subtracted from the model considering burning. Top to bottom panels show burning differences for: (**a**) all land classes, (**b**) grassland, (**c**) savanna, and (**d**) cropland.

To take the amount of monthly fire distribution into account, MODIS MOD14/MYD14 fire count data were compared to water cycle indicators using general linear least squares regression analysis (Figure 7). Correlations between annual burning changes to water balance parameters were negative. This matches findings by Ichoku [21], and supports the idea that with increased severity of fire, there is a severe decrease in hydrologic parameters including precipitation.
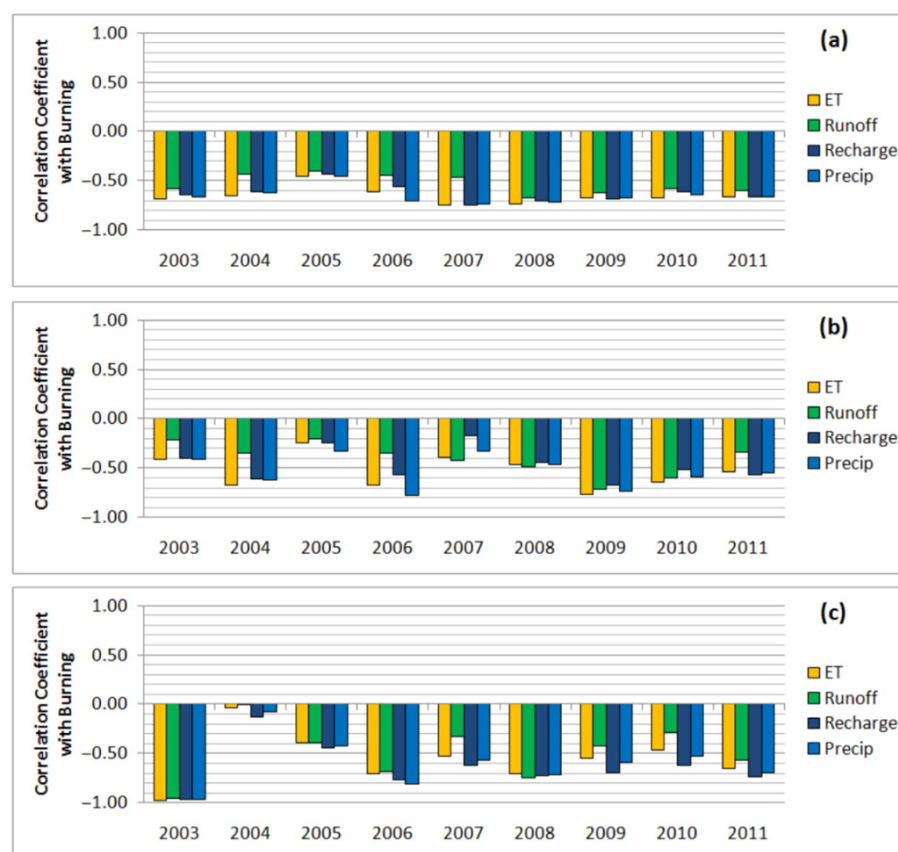
Figure 7. Correlation coefficients between biomass burning count (each count being 2 km × 2 km pixel) from MOD14/MYD14 Collection 5 compared to water balance model outputs, considering burning based on different time periods: (**a**) integration or averaging through the full-year cycle, (**b**) integration or averaging through only the dry season, and (**c**) integration or averaging through only the wet season.

To minimize the effects of quantitative biases and uncertainties, correlations between fire count and water cycle parameters were calculated for the dry season and wet season. Both seasons showed a consistent negative correlation between fire count and water cycle parameters. The dry season findings differed from what was found in the Ichoku [21] study. However, it should be noted that the study area of their entire North Central block included significant wetland converted to agriculture, especially near the LCB. The CLC has very little wetland, making up a mere 0.2% of total land coverage; the majority of wetlands in the LCB lie to the northwest of this area. Therefore, it is reasonable to presume that changes due to wetland conversion to cropland mentioned by Ichoku [21] would not be observed, because the land cover is different in this regard. Results from a scatter plot of fire count against precipitation for the CLC show that burning has an inverse relationship with precipitation [Figure 8]. The results look remarkably similar to those found by Ichoku [21], and further emphasize the inverse relationship between burning and monsoonal rainfall.
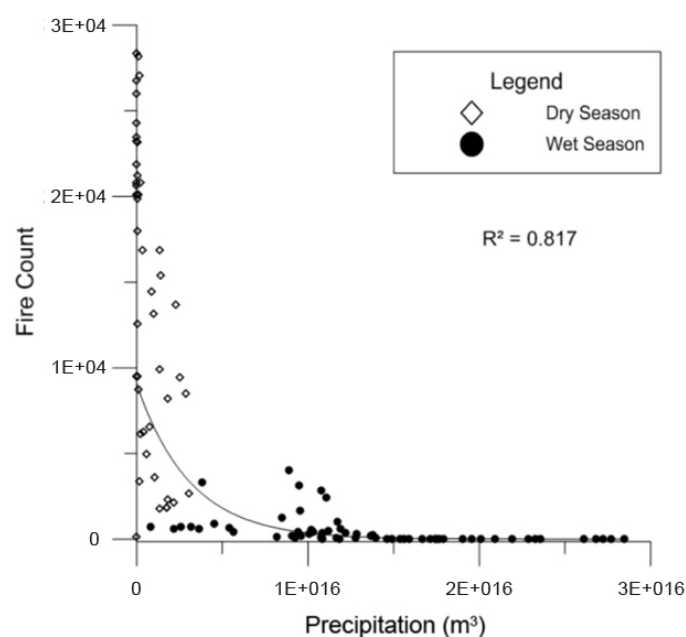
Figure 8. Scatter plot of monthly biomass burning count against precipitation from TRMM showing the demarcation between the wet season and dry season.

5. Discussion

When comparing model simulations with and without fire activity considerations, a clear pattern of decreased ET was observed in the burning model. However, lower ET may limit the amount of water available for precipitation and could have significant meteorological impacts on agriculture, although more study in this area is needed. Burning seems to also have impact on the primary land cover types of the CLC, which, in turn, significantly impacted the hydrological parameters. Analysis of the burning scenario showed that burning grassland, which comprises almost 75% of Chari–Logone total land cover, causes increased ET and runoff during the winter months. Recent studies have demonstrated an increasing trend in the LCB of converting shrubland, grassland, and wetlands to cropland. This change from grassland to cropland has the potential of decreasing water availability for water bodies during the winter.

It is known that surface runoff tends to increase on burned bare surfaces after fire due to a decrease in infiltration into soils caused by a reduction in vegetation-induced roughness and an increase in the water repellency of soils [25,26]. Vadlonga et al. [80] showed that plots with increased prescribed burning had a tendency to decrease storage capacity with no significant increase in surface runoff. However, Onda et al. [81] found that ash layers from burning clogged the preferential flow paths of rainwater, leading to a significant increase in surface runoff. With an increase in accumulated ash towards the end of the dry season burning regimen, it is reasonable to expect that precipitation would likewise not infiltrate well into the soil instead running off the surface and contributing to river flow. Therefore, fires can contribute to the intra-annual irregularity of river flow at the end of the dry season and even during the wet season. Figure 6 shows the increase in runoff with burning from all three classes at the end of the dry season and the beginning of the wet season. To fully address the intra-annual irregularity of river flow, more studies are needed, using river flow models with more discharge data.

The ability of WetSpass-M to approximate discharge found in situ shows great promise for using it to calculate hydrological parameters despite a severe lack of data. By the use of satellite data in lieu of meteorological station records, temporal and spatial limitations may be mitigated. Development of a system to incorporate albedo into PET calculations at a relatively high resolution may prove useful for future studies examining the impact of burning on albedo and land cover type, as well as on the hydrological cycle.

6. Conclusions

Burning and no-burning models were used in WetSpass-M to determine the effect of burning on land classes. The effect of burning varied by vegetative type and whether the burning occurred during the dry or wet season in the LCB. A negative correlation of fire to water cycle was clearly observed. Water balance is affected by land cover, with each land cover responding differently to burning. If the pattern of converting shrubland to cropland continues, the primary difference will be less groundwater recharge. Grassland constitutes the majority of land cover in the CLC; therefore, it is worth noting that burning increases ET and recharge during the dry season but decreases ET and recharge during the wet season. These parameters cause an increase in runoff during the wet season. This research provides insight into how burning affects different land use types within a critical region of the LCB, which provides a significant amount of water to Lake Chad. All vegetative classes in burning scenarios showed a decrease in ET during the wet season.

Further research detailing the groundwater recharge along the Chari and Logone rivers would be beneficial to understanding the hydrology of the CLC in relation to fire, but more detailed field data for rainfall and wind are probably needed, as well as groundwater measurements. A greater distribution of these measurements increasing in number near the confluence of the Chari and Logone rivers and near their combined discharge to Lake Chad would be beneficial. If more data for burning to non-burning albedo comparisons become available, a longer study period could allow for better analysis of the effect of land cover change on burning in the CLC.

References

1. Okonkwo, C.; Demoz, B.; Sakai, R.; Ichoku, C.; Anarado, C.; Adegoke, J.; Amadou, A.; Abdullahi, S.I. Combined effect of El Niño southern oscillation and Atlantic multidecadal oscillation on Lake Chad level variability. *Cogent Geosci.* **2015**, *1*. [CrossRef]
2. Musa, I.K. Saving Lake Chad. Proceedings of Sirte Roundtable. Available online: http://afrwg.icidonline.org/save_lakechad.pdf (accessed on 14 April 2021).
3. Sarch, M.T. Fishing and farming at Lake Chad: Institutions for access to natural resources. *J. Environ. Manag.* **2001**, *62*, 185–199. [CrossRef]
4. Kimmage, K.; Adams, W.M. Wetland agricultural production and river basin development in the Hadejia-Jama'are Valley, Nigeria. *Geogr. J.* **1992**, *158*, 1–12. [CrossRef]
5. Food and Agricultural Organization. Adaptive water management in the Lake Chad Basin: Addressing current challenges and adapting to future needs. In Proceedings of the Water Seminar Proceedings, World Water Week, Stockholm, Sweden, 16–22 August 2009; pp. 10–19.
6. Babamaaji, R.A.; Lee, J. Land use/land cover classification of the vicinity of Lake Chad using NigeriaSat-1 and Landsat data. *Environ. Earth Sci.* **2014**, *71*, 4309–4317. [CrossRef]

7. Bouchez, C.; Goncalves, J.; Deschamps, P.; Vallet-Coulomb, C.; Hamelin, B.; Doumnang, J.-C.; Sylvestre, F. Hydrological, chemical, and isotopic budgets of Lake Chad: A quantitative assessment of evaporation, transpiration and infiltration fluxes. *Hydrol. Earth Syst. Sci.* **2016**, *20*, 1599–1619. [CrossRef]

8. Nicholson, S.E. The West African Sahel: A review of recent studies on the rainfall regime and its interannual variability. *ISRN Meteorol.* **2013**, *2013*, 1–32. [CrossRef]

9. Nicholson, S.E.; Some, B.; Kone, B. An analysis of recent rainfall conditions in West Africa, including the rainy seasons of the 1997 El Niño and the 1998 La Niña Years. *J. Clim.* **2000**, *13*, 2628–2640. [CrossRef]

10. Policelli, F.; Hubbard, A.; Jung, H.C.; Zaitchik, B.; Ichoku, C. Lake Chad total surface water area as derived from land surface temperature andradar remote sensing data. *Remote Sens.* **2018**, *10*, 252. [CrossRef]

11. Thonicke, K.; Venevsky, S.; Sitch, S.; Cramer, W. The role of fire disturbance for global vegetation dynamics: Coupling fire into a dynamic global vegetation model. *Glob. Ecol. Biogeogr.* **2001**, *10*, 661–677. [CrossRef]

12. Lyons, E.; Jin, Y.; Randerson, J. Changes in surface albedo after fire in boreal forest ecosystems of interior Alaska assessed using MODIS satellite observations. *J. Geophys. Res.* **2008**, *113*, G02012. [CrossRef]

13. Bowman, D.; Balch, J.; Artaxo, P.; Bond, W.; Carlson, J.; Cochrane, M.; Pyne, S. Fire in the earth system. *Science* **2009**, *324*, 481–484. [CrossRef]

14. Ichoku, C.; Ellison, L. Global top-down smoke-aerosol emissions estimation using satellite fire radiative power measurements. *Atmos. Chem. Phys. Discuss.* **2014**, *14*, 6643–6667. [CrossRef]

15. van der Werf, G.R.; Randerson, J.T.; Giglio, L.; Collatz, G.J.; Mu, M.; Kasibhatla, P.S.; van Leeuwen, T.T. Global fire emissions and the contribution of deforestation, savanna, forest, agricultural, and peat fires (1997–2009). *Atmos. Chem. Phys.* **2010**, *10*, 11707–11735. [CrossRef]

16. Gatebe, C.K.; Ichoku, C.M.; Poudyal, R.; Román, M.O.; Wilcox, E. Surface albedo darkening from wildfires in Northern Sub-Saharan Africa. *Environ. Res. Lett.* **2014**, *9*, 065003. [CrossRef]

17. De Sales, F.; Xue, Y.; Okin, G.S. Impact of burned areas on the northern African seasonal climate from the perspective of regional modeling. *Clim. Dyn.* **2016**, *47*, 3393–3413. [CrossRef]

18. Dintwe, K.; Okin, G.S.; Xue, Y. Fire-induced albedo change and surface radiative forcing in sub-Saharan Africa savanna ecosystems: Implications for the energy balance. *J. Geophys. Res.* **2017**, *122*, 6186–6201. [CrossRef]

19. Atchley, A.L.; Kinoshita, A.M.; Lopez, S.R.; Trader, L.; Middleton, R. Simulating surface and subsurface water balance changes due to burn severity. *Vadose Zone J.* **2018**, *17*, 180099. [CrossRef]

20. Hodnebrog, Ø.; Myhre, G.; Forster, P.M.; Sillmann, J.; Samset, B.H. Local biomass burning is a dominant cause of the observed precipitation reduction in southern Africa. *Nat. Commun.* **2016**, *7*, 11236. [CrossRef]

21. Ichoku, C.; Ellison, L.T.; Willmot, K.E.; Matsui, T.; Dezfuli, A.K.; Gatebe, C.K.; Wang, J.; Wilcox, E.; Lee, J.; Adegoke, J.; et al. Biomass burning, land-cover change, and the hydrological cycle in Northern sub-Saharan Africa. *Environ. Res. Lett.* **2016**, *11*, 095005. [CrossRef]

22. Govaerts, Y.M. Impact of fires on surface albedo dynamics over the African continent. *J. Geophys. Res. Space Phys.* **2002**, *107*, 4629. [CrossRef]

23. Myhre, G.; Berntsen, T.K.; Govaerts, Y.; Haywood, J.M.; Lattanzio, A. Radiative effect of surface albedo change from biomass burning. *Geophys. Res. Lett.* **2005**, *32*. [CrossRef]

24. Saha, M.V.; D'Odorico, P.; Scanlon, T.M. Albedo changes after fire as an explanation of fire-induced rainfall suppression. *Geophys. Res. Lett.* **2017**, *44*, 3916–3923. [CrossRef]

25. De Bano, L.F. *Water Repellent Soils: A State-of-the-Art*; General Technical Report, (PSW-46); US Department of Agriculture, Forest Service: Washington, DC, USA, 1989.

26. Rulli, M.C.; Offeddu, L.; Santini, M. Modeling post-fire water erosion mitigation strategies. *Hydrol. Earth Syst. Sci.* **2013**, *17*, 2323–2337. [CrossRef]

27. Nyman, P.; Smith, H.; Sherwin, C.B.; Langhans, C.; Lane, P.N.; Sheridan, G. Predicting sediment delivery from debris flows after wildfire. *Geomorphology* **2015**, *250*, 173–186. [CrossRef]

28. Buma, W.G.; Lee, S.-I.; Seo, J.Y. Hydrological evaluation of Lake Chad basin using space borne and hydrological model observations. *Water* **2016**, *8*, 205. [CrossRef]

29. Ndehedehe, C.E.; Awange, J.L.; Kuhn, M.; Agutu, N.O.; Fukuda, Y. Climate teleconnections influence on West Africa's terrestrial water storage. *Hydrol. Process.* **2017**, *31*, 3206–3224. [CrossRef]

30. Ramillien, G.; Frappart, F.; Seoane, L. Application of the regional water mass variations from GRACE satellite gravimetry to large-scale water management in Africa. *Remote Sens.* **2014**, *6*, 737977–867405. [CrossRef]

31. Skaskevych, A.; Lee, J.; Jung, H.C.; Bolten, J.; David, J.L.; Policelli, F.S.; Goni, I.B.; Favreau, G.; San, S.; Ichoku, C.M. Application of GRACE to the estimation of groundwater storage change in a data-poorregion: A case study of Ngadda catchment in the Lake Chad Basin. *Hydrol. Process.* **2020**, *34*, 941–955. [CrossRef]

32. Eklund, L.; Romankiewicz, C.; Brandt, M.; Doevenspeck, M.; Samimi, C. Data and methods in the environment-migration nexus: A scale perspective. *Erde* **2016**, *147*, 139–152. [CrossRef]

33. Sanogo, S.; Fink, A.H.; Omotosho, J.A.; Ba, A.; Redl, R.; Ermert, V. Spatio-temporal characteristics of the recent rainfall recovery in West Africa. *Int. J. Clim.* **2015**, *35*, 4589–4605. [CrossRef]

34. Zhang, W.; Brandt, M.; Guichard, F.; Tian, Q.; Fensholt, R. Using long-term daily satellite based rainfall data (1983–2015) to analyze spatio-temporal changes in the sahelian rainfall regime. *J. Hydrol.* **2017**, *550*, 427–440. [CrossRef]

35. Batelaan, O.; De Smedt, F. GIS-based recharge estimation by coupling surface–subsurface water balances. *J. Hydrol.* **2007**, *337*, 337–355. [CrossRef]

36. Abdollahi, K.; Bashir, I.; Verbeiren, B.; Harouna, M.R.; Van Griensven, A.; Huysmans, M.; Batelaan, O. A distributed monthly water balance model: Formulation and application on Black Volta Basin. *Environ. Earth Sci.* **2017**, *76*, 198. [CrossRef]

37. Gao, H.; Bohn, T.; Podest, E.; McDonald, K.C.; Lettenmaier, D.P. On the causes of the shrinking of Lake Chad. *Environ. Res. Lett.* **2011**, *6*, 034021. [CrossRef]

38. Vuillaume, G. Bilanhydrologiquemensuel et modélisationsommaire du régime hydrologique du lac Tchad. Paris. Cah. ORSTOM. *Série Hydrol.* **1981**, *18*, 23–72, ISSN 0008-0381.

39. Candela, L.; Elorza, F.J.; Tamoh, K.; Jiménez-Martínez, J.; Aureli, A. Groundwater modelling with limited data sets: The Chari-Logone area (Lake Chad Basin, Chad). *Hydrol. Process.* **2014**, *28*, 3714–3727. [CrossRef]

40. Bouché, P.; Douglas-Hamilton, I.; Wittemyer, G.; Nianogo, A.J.; Doucet, J.-L.; Lejeune, P.; Vermeulen, C. Will elephants soon disappear from west African Savannahs? *PLoS ONE* **2011**, *6*, e20619. [CrossRef]

41. Seguis, L.; Cappelaere, B.; Milesi, G.; Peugeot, C.; Massuel, S.; Favreau, G. Simulated impacts of climate change and land-clearing on runoff from a small Sahelian catchment. *Hydrol. Process.* **2004**, *18*, 3401–3413. [CrossRef]

42. Boulain, N.; Cappelaere, B.; Seguis, L.; Gignoux, J.; Peugeot, C. Hydrologic and land use impacts on vegetation growth and NPP at the watershed scale in a semi-arid environment. *Reg. Environ. Chang.* **2006**, *6*, 147–156. [CrossRef]

43. Boulain, N.; Cappelaere, B.; Seguis, L.; Favreau, G.; Gignoux, J. Water balance and vegetation change in the Sahel: A case study at the watershed scale with an eco-hydrological model. *J. Arid Environ.* **2009**, *73*, 1125–1135. [CrossRef]

44. Leduc, C.; Favreau, G.; Schroeter, P. Long-term rise in a Sahelian water-table: The Continental Terminal in South-West Niger. *J. Hydrol.* **2001**, *243*, 43–54. [CrossRef]

45. Melki, A.; Abdollahi, K.; Fatahi, R.; Abida, H. Groundwater recharge estimation under semi arid climate: Case of Northern Gafsa watershed, Tunisia. *J. Afr. Earth Sci.* **2017**, *132*, 37–46. [CrossRef]

46. Li, M.; Shao, Q. An improved statistical approach to merge satellite rainfall estimates and raingauge data. *J. Hydrol.* **2010**, *385*, 51–64. [CrossRef]

47. Pombo, S.M.; de Oliveira, R.P. Evaluation of extreme precipitation estimates from TRMM in Angola. *J. Hydrol.* **2015**, *523*, 663–679. [CrossRef]

48. Ojo, J.; Omotosho, T. Comparison of 1-min rain rate derived from TRMM satellite data and raingauge data for microwave applications in Nigeria. *J. Atmos. Sol. Terr. Phys.* **2013**, *102*, 17–25. [CrossRef]

49. Friedl, M.A.; McIver, D.K.; Hodges, J.C.; Zhang, X.; Muchoney, D.; Strahler, A.H.; Cooper, A. Global land covermapping from MODIS: Algorithms and early results. *Remote Sens. Environ.* **2002**, *83*, 287–302. [CrossRef]

50. Friedl, M.A.; Sulla-Menashe, D.; Tan, B.; Schneider, A.; Ramankutty, N.; Sibley, A.; Huang, X. MODIS collection 5 global land cover: Algorithm refinements and characterization of new datasets. *Remote Sens. Environ.* **2010**, *114*, 168–182. [CrossRef]

51. Al-Hamdan, M.Z.; Oduor, P.; Flores, A.I.; Kotikot, S.M.; Mugo, R.; Ababu, J.; Farah, H. Evaluating land cover changes in Eastern and Southern Africa from 2000 to 2010 using validated Landsat and MODIS data. *Int. J. Appl. Earth Obs. Geoinf.* **2017**, *62*, 8–26. [CrossRef]

52. Gessner, U.; Bliefernicht, J.; Rahmann, M.; Dech, S. Land cover maps for regional climate modeling in West Africa—A comparison of datasets. In Proceedings of the 32nd Annual EARSeL Symposium, Mykonos, Greece, 21–25 May 2012.

53. Vintrou, E.; Desbrossea, A.; Beguea, A.; Traoreb, S.; Barona, C.; Seena, D. Crop area mapping in West Africa using landscape stratification of MODIS time series and comparison with existing global land products. *Int. J. Appl. Earth Obs. Geoinf.* **2012**, *14*, 83–93. [CrossRef]

54. Yang, Y.; Xiao, P.; Feng, X.; Li, H. Accuracy assessment of seven global land cover datasets over China. *ISPRS J. Photogramm. Remote Sens.* **2017**, *125*, 156–173. [CrossRef]

55. Giglio, L.; Descloitres, J.; Justice, C.O.; Kaufman, Y.J. An enhanced contextual fire detection algorithm for MODIS. *Remote Sens. Environ.* **2003**, *87*, 273–282. [CrossRef]

56. Justice, C.; Giglio, L.; Korontzi, S.; Owens, J.; Morisette, J.; Roy, D.; Descloitres, J.; Alleaume, S.; Petitcolin, F.; Kaufman, Y. The MODIS fire products. *Remote Sens. Environ.* **2002**, *83*, 244–262. [CrossRef]

57. Schulze, E.-D. Short-term and long-term effects of plant water deficits on stomatal response to humidity in *Corylus avellana* L. *Planta* **1979**, *146*, 319–326. [CrossRef] [PubMed]

58. Li, F.; Lawrence, D.M.; Bond-Lamberty, B. Human impacts on 20th century fire dynamics and implications for global carbon and water trajectories. *Glob. Planet. Chang.* **2018**, *162*, 18–27. [CrossRef]

59. Bosilovich, M.G. A comparison of MODIS land surface temperature with in situ observations. *Geophys. Res. Lett.* **2006**, *33*. [CrossRef]

60. Coll, C.; Wan, Z.; Galve, J.M. Temperature-based and radiance-based validations of the V5 MODIS land surface temperature product. *J. Geophys. Res. Space Phys.* **2009**, *114*. [CrossRef]

61. Wan, Z.; Li, Z. Radiance-based validation of the V5 MODIS land-surface temperature product. *Int. J. Remote Sens.* **2008**, *29*, 5373–5395. [CrossRef]

62. Hulley, G.C.; Hook, S.J. Intercomparison of versions 4, 4.1 and 5 of the MODIS Land Surface Temperature and Emissivity products and validation with laboratory measurements of sand samples from the Namib desert, Namibia. *Remote Sens. Environ.* **2009**, *113*, 1313–1318. [CrossRef]

63. Engelstaedter, S.; Washington, R. Evaluation of reanalysis near-surface winds over northern Africa in Boreal summer. In *EGU General Assembly Conference Abstracts*; EGU General Assembly: Vienna, Austria, 2014; p. 13169.

64. Mughal, M.; Lynch, M.; Yu, F.; McGann, B.; Jeanneret, F.; Sutton, J. Wind modelling, validation and sensitivity study using Weather Research and Forecasting model in complex terrain. *Environ. Model. Softw.* **2017**, *90*, 107–125. [CrossRef]

65. Oliver, M.A.; Webster, R. Kriging: A method of interpolation for geographical information systems. *Int. J. Geogr. Inf. Syst.* **1990**, *4*, 313–332. [CrossRef]

66. Yu, X.; Lu, C. Urban percent impervious surface and its relationship with land surface temperature in Yantai City, China. *IOP Conf. Ser. Earth Environ. Sci.* **2014**, *17*, 7. [CrossRef]

67. Valiantzas, J.D. Simplified versions for the Penman evaporation equation using routine weather data. *J. Hydrol.* **2006**, *331*, 690–702. [CrossRef]

68. Vegetation and hydrology. H. L. Penman (Technical Communication No. 53, Commonwealth Bureau of Soils, Harpenden) Commonwealth Agricultural Bureaux, Farham Royal, 1963. Pp. v, 124: 72 Tables. 20s. Available online: https://ui.adsabs.harvard.edu/abs/1963QJRMS..89..565./abstract (accessed on 9 May 2021).

69. Shuttleworth, W.J. Evaporation. In *Maidment*; McGraw-Hill: New York, NY, USA, 1993; pp. 4.1–4.53.

70. Allen, R.G.; Smith, M.; Pereira, L.S.; Perrier, A. An update for the calculation of reference evapotranspiration. *ICID Bull.* **1994**, *43*, 35–92.

71. Zomer, R.J.; Bossio, D.A.; Trabucco, A.; Yuanjie, L.; Gupta, D.C.; Singh, V.P. *Trees and Water: Smallholder Agroforestry on Irrigated Lands in Northern India. Colombo, Sri Lanka*; IWMI Research Report; International Water Management Institute: Cairo, Egypt, 2007; p. 45.

72. Zomer, R.J.; Trabucco, A.; Bossio, D.A.; van Straaten, O.; Verchot, L.V. Climate change mitigation: A spatial analysis of global land suitability for clean development mechanism afforestation and reforestation. *Agric. Ecosyst. Environ.* **2008**, *126*, 67–80. [CrossRef]

73. van Zyl, J.J. The Shuttle Radar Topography Mission (SRTM): A breakthrough in remote sensing of topography. *Acta Astronaut* **2001**, *48*, 559–565. [CrossRef]

74. Sun, G.; Ranson, K.; Kharuk, V.; Kovacs, K. Validation of surface height from shuttle radar topography mission using shuttle laser altimeter. *Remote Sens. Environ.* **2003**, *88*, 401–411. [CrossRef]

75. Federal Institute of Geosciences and Natural Resources & Lake Chad Commission. Lake Chad Sustainable Water Management Project Activities—Report N° 3. 2010. Available online: https://www.whymap.org/EN/Themen/Wasser/Projekte/abgeschlossen/TZ/Tschad/report_3.pdf?__blob=publicationFile&v=3 (accessed on 4 February 2019).

76. Seeber, K. *2nd Mission on Discharge Measurements at Chari, Logone and Koulambou River, Chad*; Federal Ministry for Economic Cooperation and Development: Hanovra, Germany, 2013.

77. Oliver FC &Singels, A. The effect of crop residue layers on evapotranspiration, growth and yield of irrigated sugarcane. *Water SA* **2012**, *38*, 77–86.

78. Moriasi, D.N.; Gitau, M.W.; Pai, N.; Daggupati, P. Hydrologic and water quality models: Performance measures and evaluation criteria. *Trans. ASABE* **2015**, *58*, 1763–1785. [CrossRef]

79. Notaro, M.; Wyrwoll, K.-H.; Chen, G. Did aboriginal vegetation burning impact on the Australian summer monsoon? *Geophys. Res. Lett.* **2011**, *38*. [CrossRef]

80. Vadilonga, T.; Úbeda, X.; Germann, P.F.; Lorca, M. Effects of prescribed burnings on soil hydrological parameters. *Hydrol. Process.* **2008**, *22*, 4249–4256. [CrossRef]

81. Onda, Y.; Dietrich, W.E.; Booker, F. Evolution of overland flow after a severe forest fire, Point Reyes, California. *Catena* **2008**, *72*, 13–20. [CrossRef]